



LAWRENCE
LIVERMORE
NATIONAL
LABORATORY

Pre-shot simulations of far-field ground motion for the Source Physics Experiment (SPE) Explosions at the Climax Stock, Nevada National Security Site: SPE2

R. J. Mellors, A. Rodgers, W. Walter, S. Ford, H. Xu, E. Matzel, S. Myers, N. A. Petersson, B. Sjogreen, T. Hauk, J. Wagoner

October 20, 2011

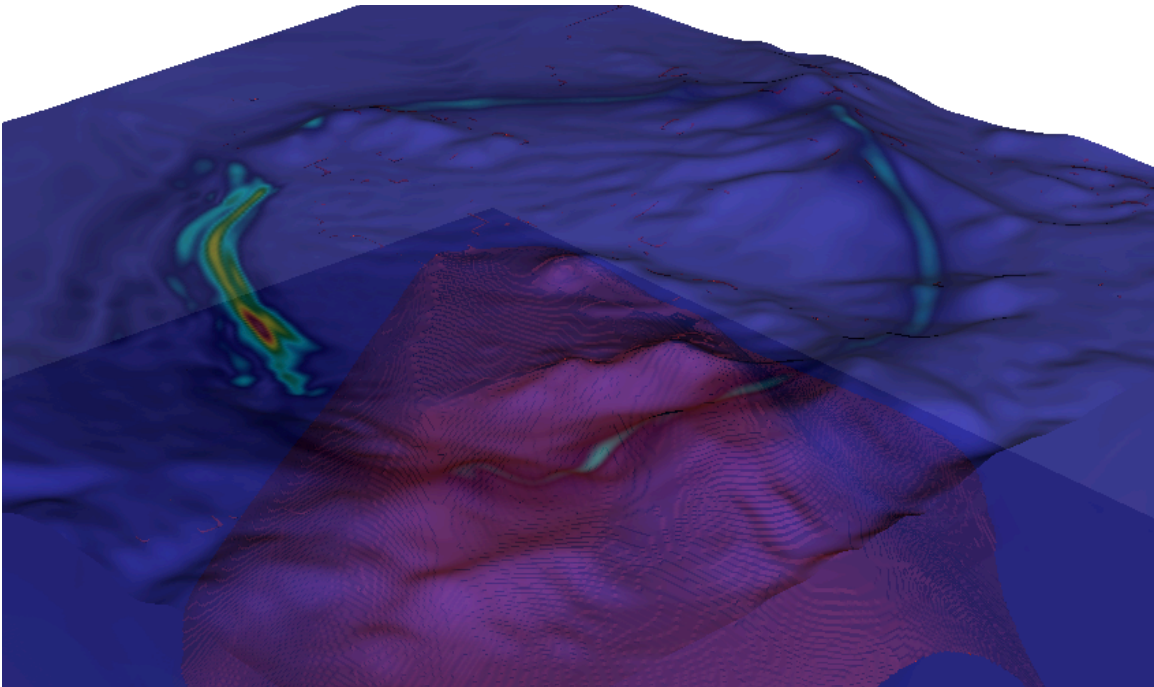
Disclaimer

This document was prepared as an account of work sponsored by an agency of the United States government. Neither the United States government nor Lawrence Livermore National Security, LLC, nor any of their employees makes any warranty, expressed or implied, or assumes any legal liability or responsibility for the accuracy, completeness, or usefulness of any information, apparatus, product, or process disclosed, or represents that its use would not infringe privately owned rights. Reference herein to any specific commercial product, process, or service by trade name, trademark, manufacturer, or otherwise does not necessarily constitute or imply its endorsement, recommendation, or favoring by the United States government or Lawrence Livermore National Security, LLC. The views and opinions of authors expressed herein do not necessarily state or reflect those of the United States government or Lawrence Livermore National Security, LLC, and shall not be used for advertising or product endorsement purposes.

This work performed under the auspices of the U.S. Department of Energy by Lawrence Livermore National Laboratory under Contract DE-AC52-07NA27344.

**Pre-shot simulations of far-field ground motion for the Source
Physics Experiment (SPE) Explosions at the Climax Stock, Nevada
National Security Site: SPE2**

R. J. Mellors, A. J. Rodgers, W. R. Walter, S. Ford, H. Xu, E. Matzel, S. Myers, N. A.
Pettersson, B. Sjogreen, T. Hauk, and J. Wagoner



Summary. The Source Physics Experiment (SPE) is planning a 1000 kg (TNT equivalent) shot (SPE2) at the Nevada National Security Site (NNSS) in a granite borehole at a depth (canister centroid) of 45 meters. This shot follows an earlier shot of 100 kg in the same borehole at a depth 60 m. Surrounding the shotpoint is an extensive array of seismic sensors arrayed in 5 radial lines extending out 2 km to the north and east and approximately 10-15 to the south and west. Prior to SPE1, simulations using a finite difference code and a 3D numerical model based on the geologic setting were conducted, which predicted higher amplitudes to the south and east in the alluvium of Yucca Flat along with significant energy on the transvers components caused by scattering within the 3D volume along with some contribution by topographic scattering. Observations from the SPE1 shot largely confirmed these predictions although the ratio of transverse energy relative to the vertical and radial components was in general larger than predicted.

A new set of simulations has been conducted for the upcoming SPE2 shot. These include improvements to the velocity model based on SPE1 observations as well as new capabilities added to the simulation code. The most significant is the addition of a new source model within the finite difference code by using the predicted ground velocities from a hydrodynamic code (GEODYN) as driving condition on the boundaries of a cube embedded within WPP which provides a more sophisticated source modeling capability linked directly to source site materials (e.g. granite) and type and size of source. Two sets of SPE2 simulations are conducted, one with a GEODYN source and 3D complex media (no topography node spacing of 5 m) and one with a standard isotropic pre-defined time function (3D complex media with topography, node spacing of 5 m). Results were provided as time series at specific points corresponding to sensor locations for both translational (x,y,z) and rotational components.

Estimates of spectral scaling for SPE2 are provided using a modified version of the Mueller-Murphy model. An estimate of expected aftershock probabilities were also provided, based on the methodology of *Ford and Walter*, [2010].

Introduction. The Source Physics Experiment (SPE) is a research effort aimed at improving the modeling and simulation of explosions by developing a better physical understanding of the fundamental controls on wave generation and propagation. A particular focus is on shear waves, which are poorly predicted by existing explosion models, despite their important role in event identification and yield estimation. The SPE is intended as a series of chemical explosions, of varying sizes and settings, which will be recorded on extensive instrumentation located both near the source and at extended distances. One objective is to predict the waveforms prior to each shot as a test of the planned gradual improvement of predictive capability of our source and path models and codes. The first chemical shot, SPE1, (100 kg TNT equivalent at 60 m) was conducted on May 3, 2011 and a second, larger (1000 kg TNT equivalent; 1166 kg of SHANFO at 45 m centroid depth) shot is planned on Oct. 25, 2011. This report is intended to serve as a summary of the pre-shot simulation of the ‘far-field’ effects of the Oct 25, 2011 shot (SPE2). By ‘far-field’ we refer to distances at which seismic wave propagation is primarily elastic [Rodgers *et al.*, 2010].

This report summarizes some of the results from the data analysis from SPE1 [Mellors *et al.*, 2011a, b], compares the results with the pre-shot simulation, and then documents improvements in the modeling and numerical capabilities as a result of the SPE1 analysis along with new simulations and predictions for the SPE2 dataset. Improvements include a more sophisticated source based on nonlinear modeling, a refined velocity model, simulations of rotational motion, and aftershock predictions.

Geologic setting. The initial SPE shots will take place in the northeast corner of the Nevada National Security Site (NNSS) (Figure 1). The NNSS possesses a complex geologic setting with strong lateral and vertical variations in geophysical properties relevant to seismic wave propagation. The SPE1 ground zero is located in an outcrop of granite surrounded by volcanic and sedimentary rocks. The main units near the SPE site consist of the granite (Climax Stock), alluvium, Tertiary volcanic tuffs, and Pre-Tertiary sedimentary rocks (mainly carbonates). The alluvium, which is relatively low-density is thickest southwest of the shot point, in the topographically flat Yucca Flat. Yucca Flat is also notable for a deep water table, which reduces shallow seismic velocities. Northwest of the shot point the topography increases with a steep gradient and the area is dominated by pre-Tertiary carbonates. For a detailed description of NNSS geology see Howard [1985] and for the Climax Stock/ Yucca Flat area see GSG, [2006].

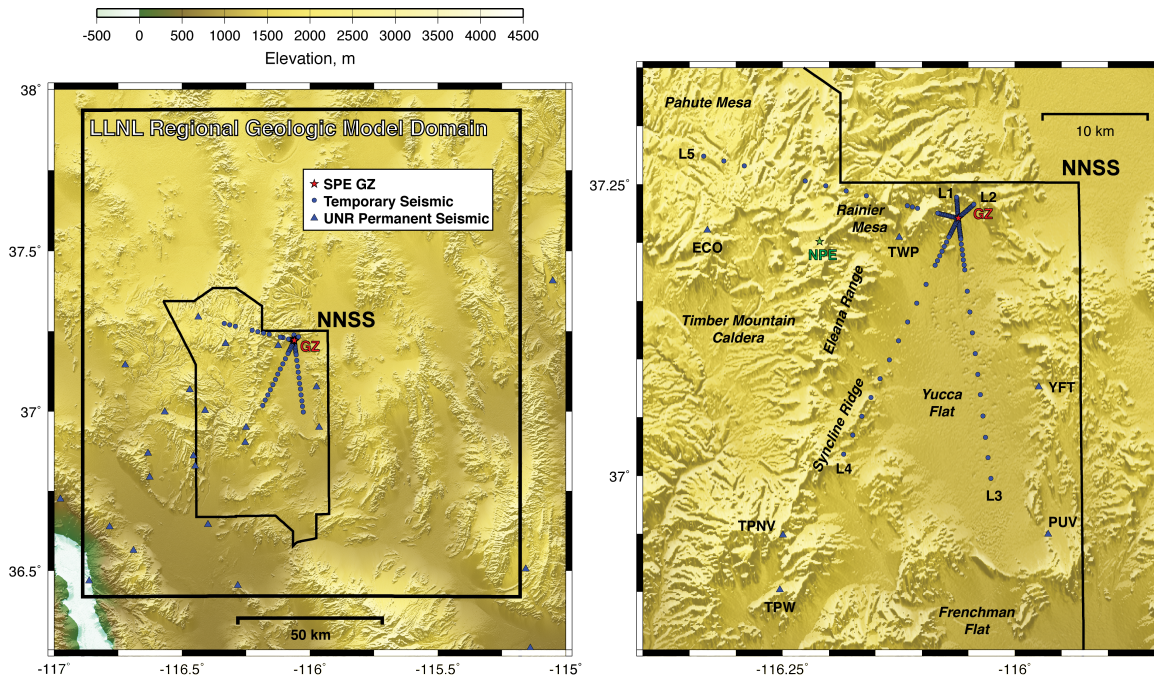


Figure 1. Map showing permanent (triangles) and temporary (circles) seismic stations that will record the first round of SPE shots along with topography. SPE ground zero is indicated by the red star. **(left)** Regional scale covering southern Nevada and the boundary of the Nevada National Security Site (NNSS). **(right)** Local scale covering the northern part of the NNSS. Note that the Non-Proliferation Experiment (NPE) ground zero is shown with a green star. From Rodgers et al. [2011].

SPE1 seismic network. The SPE1 shot was a chemical explosion of 100 kg of explosives detonated at a depth of 60 m on May 3, 2011. A comprehensive data set was collected from the SPE1 calibration shot and included over 150 instruments (Figure 1). A variety of instruments including short-period geophones (GS11d), accelerometers (Episensors), rotational sensors (eentec R1) and broad-band (CMG40 and Trilliums) were deployed (Figures 1 and 2). Most of the instruments were installed in 5 radial lines centered on the shot location, with the closest instruments spaced 100 m away. Spacing between sites was 100 m up to a distance of 2 km from the shot point. Lines 3, 4 and 5 extended further with broadband instruments located out to a distance of 10 km. Nine other sites not located on the radial lines were also occupied by either broadband or accelerometers. Data is also available from the University of Reno seismic network. Instruments are located on concrete pads set in the ground, with horizontal components oriented radially and tangentially towards the shot point (manually).

SPE1 pre-shot simulation. Prior to the SPE1 shot, a comprehensive modeling effort was undertaken and presented in Rodgers et al. [2010]. The modeling used an advanced finite-difference algorithm (WPP) [Pettersson and Sjogreen, 2009, 2010, 2011; Sjogreen and Pettersson, 2010] to conduct 3D modeling of the seismic waveforms at distance up to 8 km from the source. WPP has the capability to handle

3D variations in the material properties (density, compressional and shear wavespeed and the attenuation factor, Q) and a variety of sources including point sources and moment tensor representations. The free-surface boundary can include topography and the remaining sides of the domain include absorbing boundaries. It also includes depth-dependent mesh refinement to improve performance for models with increased wavespeeds at depth [Pettersson, 2011].

A 3D model was constructed using a set of four layers (alluvium, Tertiary, Pre-Tertiary, and granite) to represent the complex geologic setting of the SPE test site. Interfaces between layers were imported from a GIS-based geologic model of the area and based mainly on surface mapping, borehole data, and geophysical modeling. Layer depths between known points were defined by interpolation within the GIS program (Earthvision) and then reformatted to match WPP input format. Each layer interface varied laterally and homogenous material properties were assigned to each layer based on previous studies.

One problem is that the expected velocities for the alluvium may be as low as a few hundred meters per second; unfortunately, properly accounting for wave speeds this slow with the current implementation of WPP (second order) requires a very close node spacing and excessively large models and the S wave velocity was set at 1 km/s for the alluvium. Another issue is that while the geologic model is based on the best available information, alternative realizations of the geologic model exist (e.g. GSG, 2006).

Based on this geologic representation, a set of four simulations using a domain of 8 km by 8 km by 5 km with a grid spacing of 5 meters were generated. These models increased in complexity and included: 1) homogenous half-space with a flat boundary; 2) homogenous half-space with topography; 3) 3D heterogeneity with a flat boundary; and 4) 3D heterogeneity with topography. The results indicated that the 3D volumetric structure would have a pronounced effect on the ground motions, especially to the southwest as the wavefield propagated into the low velocity alluvium of Yucca Flat, where high amplitudes were generated. The effect was expected to be strongest on Lines 3 and 4. Volume scattering from heterogeneities in the velocity model caused scattering, which appears as transverse energy. This is most evident on lines 3 and 4. Some scattering due to topography was expected to the northwest.

SPE1 data. Data recovery was good, with approximately 95% return of useful data. Some anomalies were noted in recorded amplitudes for selected stations, possibly due to instrument or cable problems [Mellors *et al.*, 2011]. The amplitude anomalies caused some difficulties in comparison of predicted amplitude with observed, due to uncertainties in observed amplitudes.

Clear differences along and between lines were observed (*Figures 3, 4, and 5*), which in general matched the predictions. Lines 3 and 4 were delayed relative to the other lines and strong variations in amplitude and waveforms were observed, with pronounced surface waves visible on Lines 3 and 4. The synthetics underestimated

the relative proportion of transverse energy on lines 1 and 2. At this distance, the seismic waves traveled only through the granite (Climax Stock) for Lines 1 and 2. As it was modeled as a homogenous media, little scattering was expected. The amount of transverse energy observed in the data suggests that either the source generated the transverse energy or an unexpected amount of scattering occurred within the granite. Topographic effects were predicted but these were difficult to distinguish in the data from 3D volume effects and also possibly because the stations with expected pronounced topographic effect were not deployed along line 5 due to difficulty of access.

Systematic differences in travel times between the model and the data were also observed and in particular for the granite. A P velocity of 5.5 km/s had been used but this proved to be too high to match the first arrivals, which were presumed to be direct waves. This may be due in part to a slower velocity weathered layer, which on the basis of refraction experiments, appears to be 10-20 m thick. Unfortunately, at the scale of the modeling used in this study, including layers of this thickness (i.e. one or two nodes) is impractical.

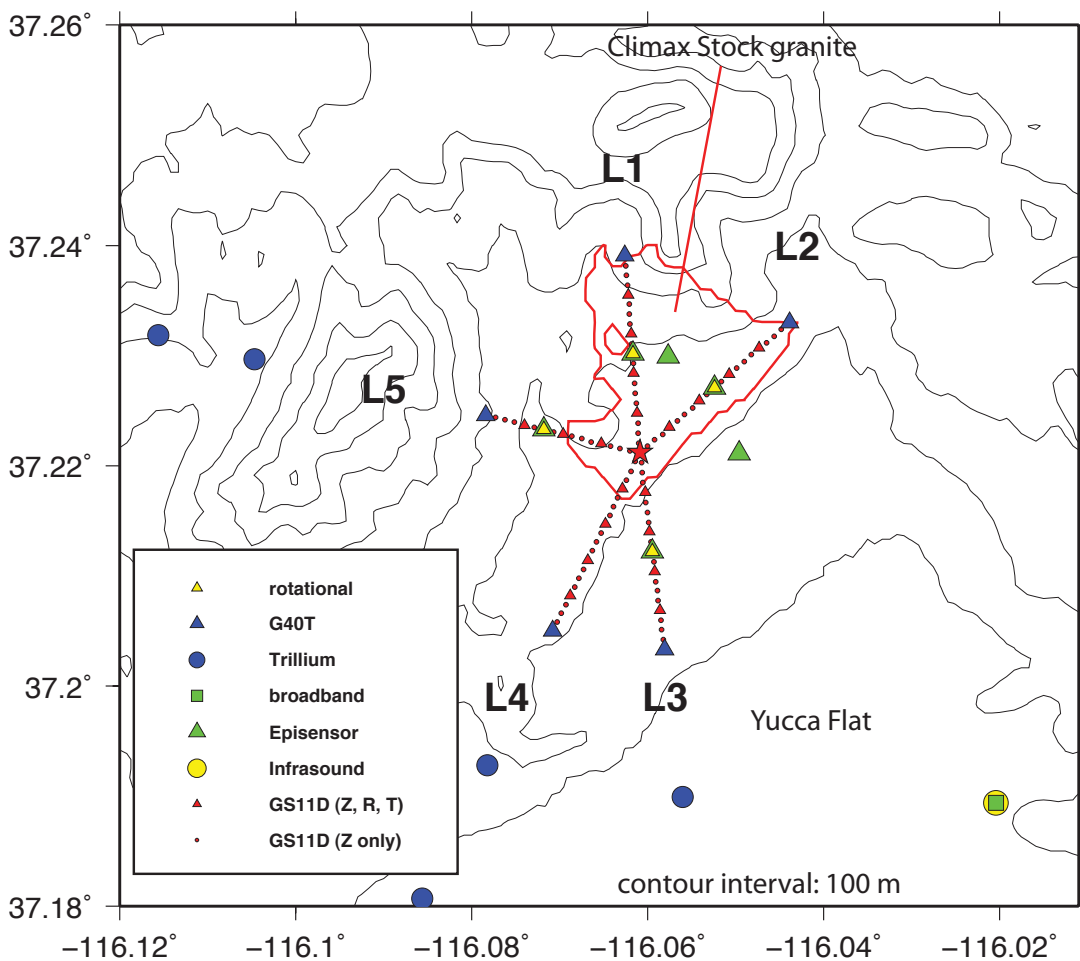


Figure 2. Map of SPE seismic network.

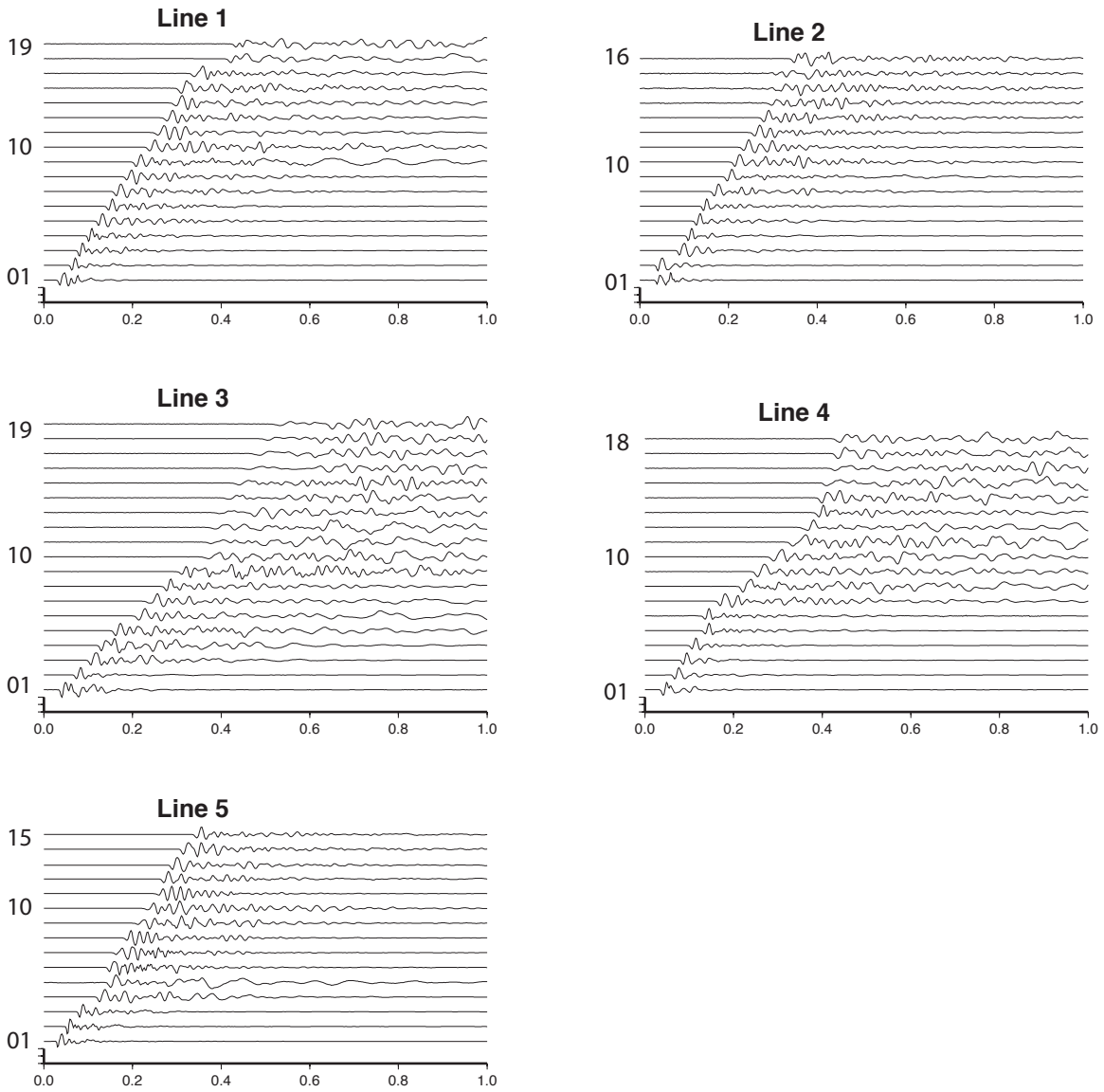


Figure 3. Seismic data (vertical component) recorded from the SPE1 shot showing stations numbers at left. Traces with high noise or instrumental problems have been omitted. Lines 1 and 2 are almost entirely within the granite while only first few stations of Lines 3 and 4 are on granite before transitioning to alluvium or Tertiary tuffs. Note changes in first arrival moveout and amplitude at a distance of approximately 1 km on Lines 3 and 4. Line 5 extends from granite to Pre-Tertiary.

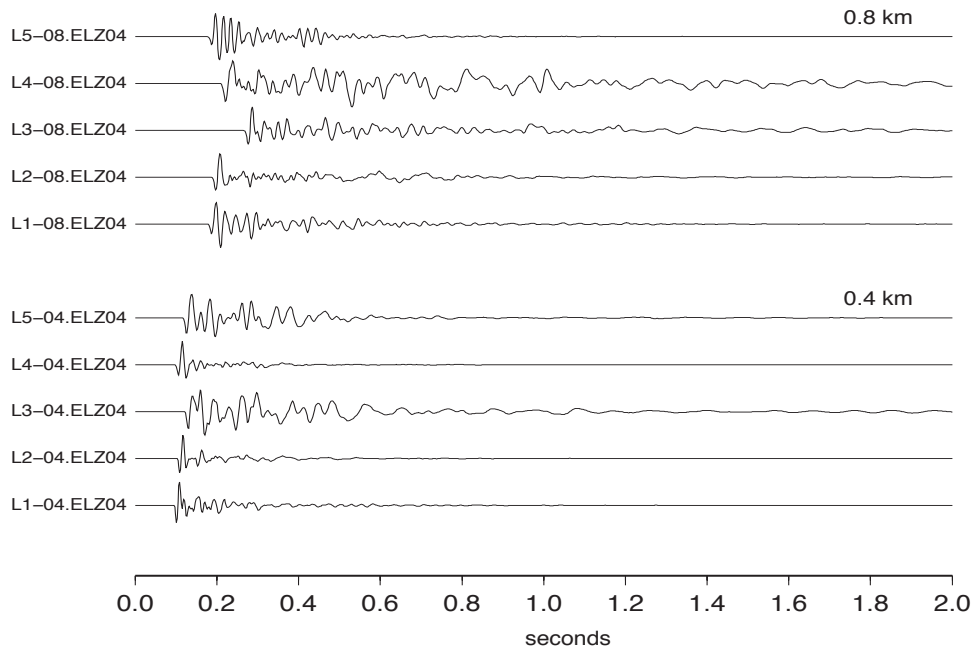


Figure 4. Seismograms (vertical) observed at 0.4 and 0.8 km from the shot location but at different azimuths. Note significant differences in traveltime and appearance.

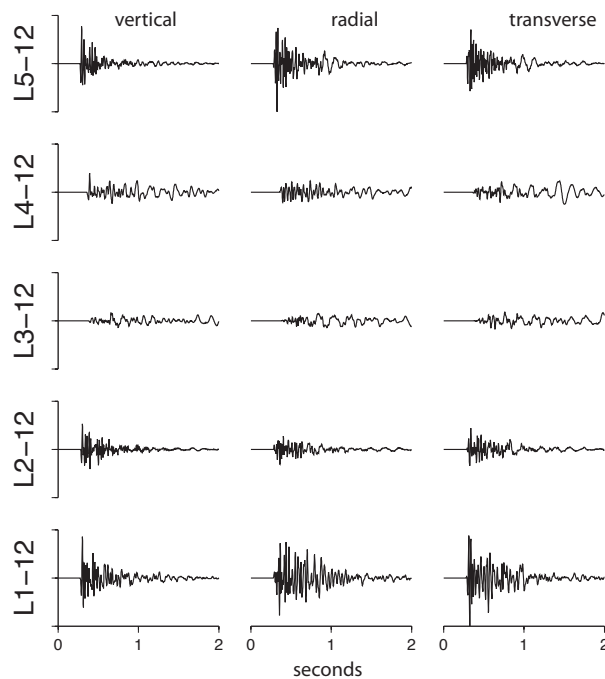


Figure 5. Vertical, radial, and transverse components of seismograms recorded at a distance of 1.2 km from the shot. Labels on the vertical axis refer to the line (L1, L2, L3, L4 and L5) and the station (12). The L3 and L4 lines show a delayed arrival and lower frequencies, as predicted.

Model improvements. The first step was to refine the velocity model. The layer boundaries, which were based on the geologic model (*Figures 6 and 7*), were retained but the material properties revised to match observed arrival times.

Based on the measured travel-times for the nearby (< 2 km) stations from the SPE1 shot using the first P arrival, P velocities for the granite, alluvium, and Tertiary tuff were modified. P arrival times were also measured for the synthetic data and compared with the observed data. The Pre-Tertiary was poorly constrained using first-arrival travel times as only parts of line 4 and 5 cross the Pre-Tertiary and hence was not modified (*Table 1*). Lines 3, 4 and 5 show indication of a change in slope in the plot of time versus distance at distances of roughly 1 km and this may reflect a refracted wave as well as changes in the uppermost layer velocity.

One curious feature is on Line 2, where the P arrival time at distance of 100 and 200 m is almost exactly the same. No obvious instrumental cause exists and it is possibly due to pronounced variations in velocity within the granite.

In parallel with this effort ambient noise cross-correlation was conducted to develop empirical Green's functions of the interstation velocity structure (*Figure 8*). This appears to be a promising approach to refining the velocity model although as of yet, insufficient data has been provided to enhance the signal-to-noise ratio sufficiently to provide robust results. At short distances (less than 300 m) the noise is highly correlated at the frequencies recorded by the GS11d geophones. At longer distances the high frequency signal is just beginning to emerge from the noise and should be well defined once more data are included in the correlation stacks. Data collected prior to the SPE2 shot should adequate to accomplish this.

While these modifications improved the fit within the granite, and to a lesser degree in the alluvium, some discrepancies remained. As inaccurate layer thicknesses as well as layer velocities may have caused these discrepancies, it was decided not to address these problems at the current time. The revised model predicted travel times within the Climax Stock well (*Figure 9*) although the fit to Lines 3 and 4 requires further adjustment. We anticipate that travel-time for SPE2 will be identical, although it is possible that refracted head waves that were previously below the noise threshold for SPE1 may become visible for SPE2 and hence produce minor variations.

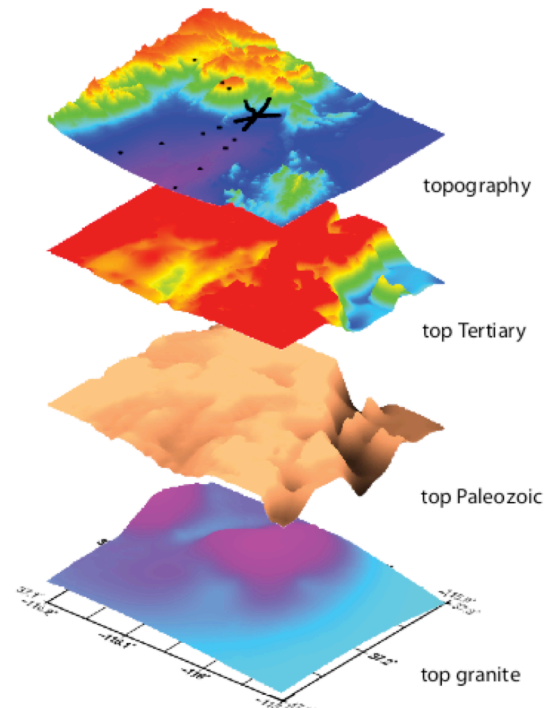


Figure 6. Perspective view of layers and boundaries.

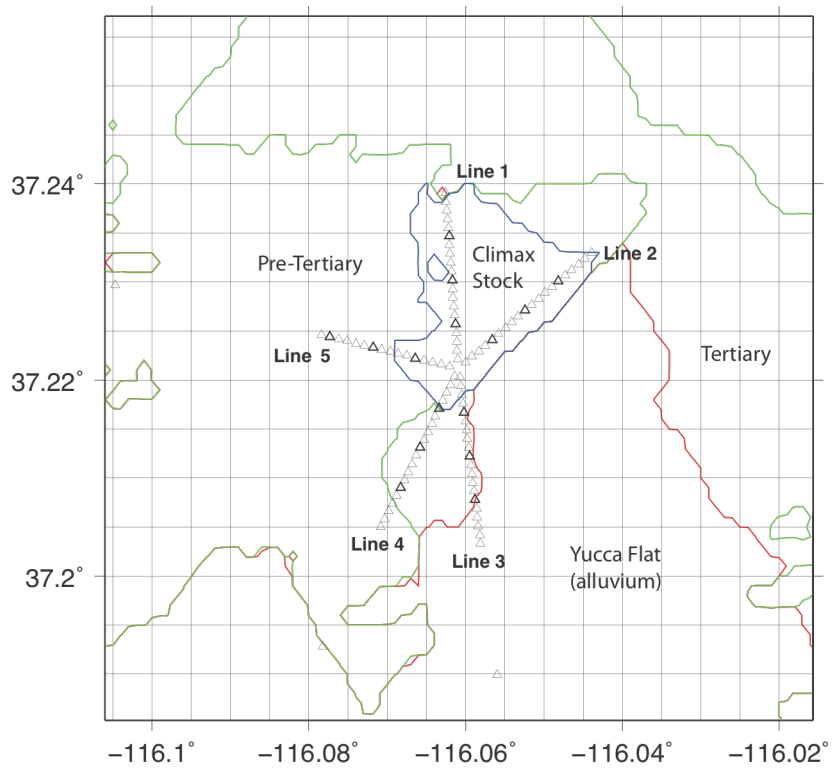


Figure 7. Map of layer boundaries and stations.

Table 1. Revised velocities.

Layer	Vp (m/s)	Vs (m/s)	Rho (kg/m ³)
alluvium	1730	1000*	2000
Tertiary Tuff	3000	1732	2100
Pre-Tertiary	4000	2312	2300
Granite	4500	2598	2600

*defined to to be 1000 m/s to avoid close nodes spacing and extremely large models.

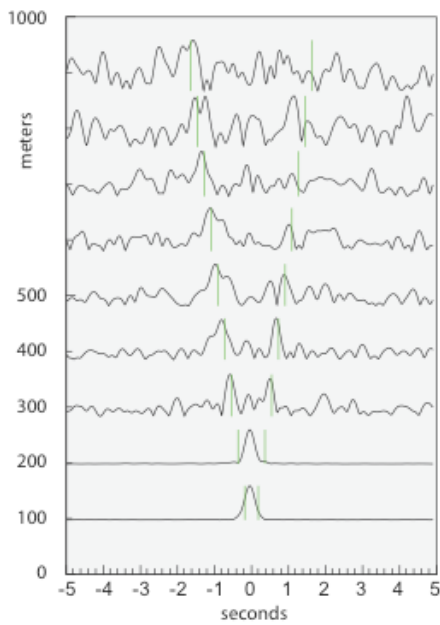


Figure 8. An example of noise cross-correlation based on data recorded by the L3 line over a period of 8 days and showing the developments of empirical Green's functions for each inter-station interval. It was filtered between 2 and 8 Hz before correlation. The red lines mark group velocities of ± 0.55 km/s to emphasize peaks.

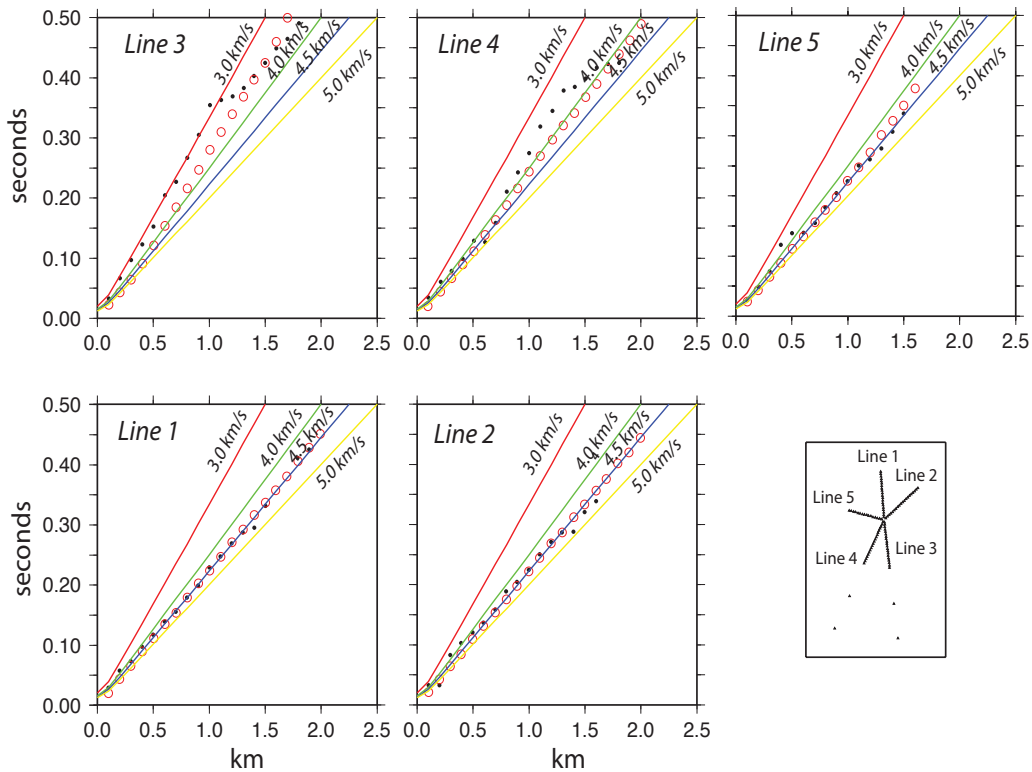


Figure 9. P first arrival travel times from data (black dots) compared with synthetic first arrival travel times (red circles) for the first 2.5 km away from the shot location for each lines. Expected travel times for a 60 m deep source in a constant velocity are shown as solid lines. Although slight differences exists between lines 1 and 2, the granite appears to be between 4.5 and 5.0 km/s, in contrast with core data, which suggests velocities as fast as 5.5 km/s. The difference may be due to a weathered layer at the surface. Velocities along line 3, which transverses alluvium, tend to be slower than predicted using the model.

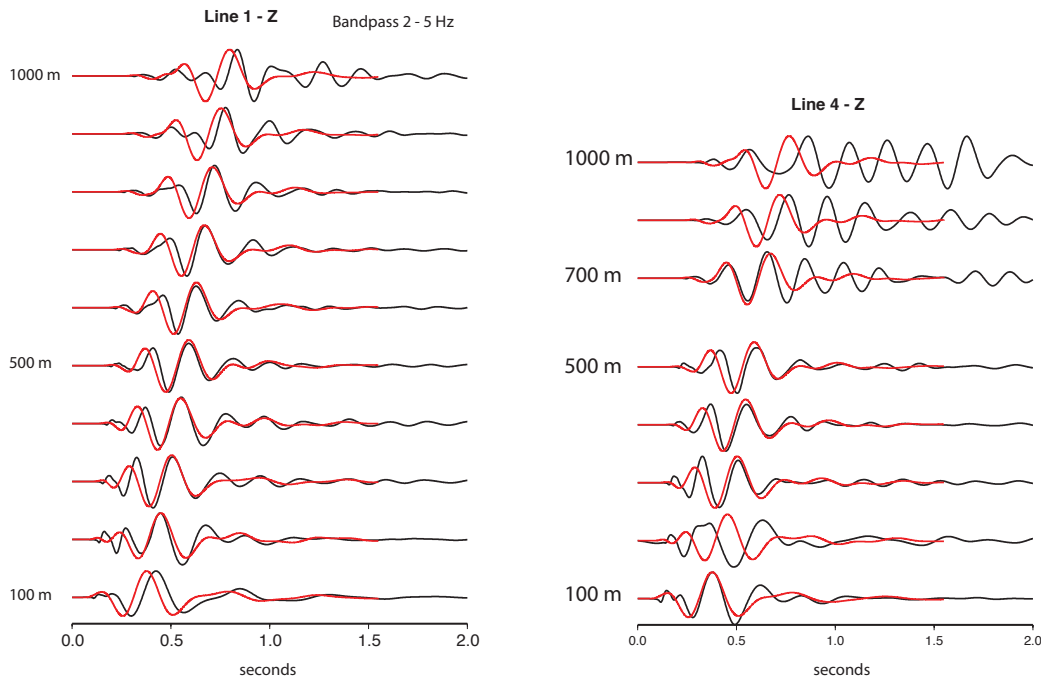


Figure 10 Middle and right show filtered (2-5 Hz) synthetics based on the revised model (red) with instrument corrected data (black) (normalized). Inside granite boundaries the fit is reasonable but poor outside.

Using the revised model, the fit between predicted and observed (SPE1) waveforms was examined (*Figure 10*). Waveform fit depends on the accuracy of the geologic model and numerical assumptions and hence generally decreases with increasing frequency and path complexity. This is true for the SPE1 waveforms, which showed an approximate match for filtered (bandpass 2 – 5 Hz) for lines 1 and 2 but poorer for lines 3-5. The observed data showed generation of surface waves at distances greater than 0.5 km along line 4 which were not generated in the synthetics. This is likely due to the artificially high (1000 m/s) shear wave velocity in the model as compared to the near surface velocities in Yucca Flat, which may be as low as 500 m/s based on borehole seismic velocity measurements (*Howard, 1985*).

SPE2 simulations. The same seismic network will be in place for the SPE2 shot and a set of simulations was conducted for the SPE2 shot assuming identical locations and instrument types as in SPE1. These simulations use the revised model and model the SPE2 waveforms for standard orthogonal motions (x,y, and z) and also for rotational motion. These simulations include two types of source parameterizations: an isotropic source and a coupled nonlinear source, calculated by a different code named GEODYN.

The GEODYN/WPP coupling (one-way) is a new capability [*Rodgers et al, 2011*] and although the coupling has been extensively tested, results presented here should be

considered preliminary. Initial experiments are intriguing and combined GEODYN/WPP models show great promise in replicating key observations such as the difference in P wave radiation between chemical and nuclear explosions and replicating the Mueller-Murphy spectral source model [Rodgers *et al.*, 2011].

GEODYN is a 3D Eulerian hydrocode [Antoun *et al.*, 2001, 2004, 2011; Antoun and Lomov, 2003; Lomov *et al.*, 2003], which simulates the hydrodynamic response of materials to explosion loading and includes the capability to handle nonlinear effects such as tensile failure and yielding [Rodgers *et al.*, 2011]. A Jones-Wilkins-Lee (JWL) equation of state is used to estimate the response of the ANFO explosive mix in the SPE1 and SPE2 shots. Velocities within a 100 m cube are generated and relayed to WPP as a driving boundary condition. The advantage of linking GEODYN with WPP is that GEODYN handles the source region accurately but is numerically expensive; WPP can extend the motions in the elastic regime where most seismic measurements are made.

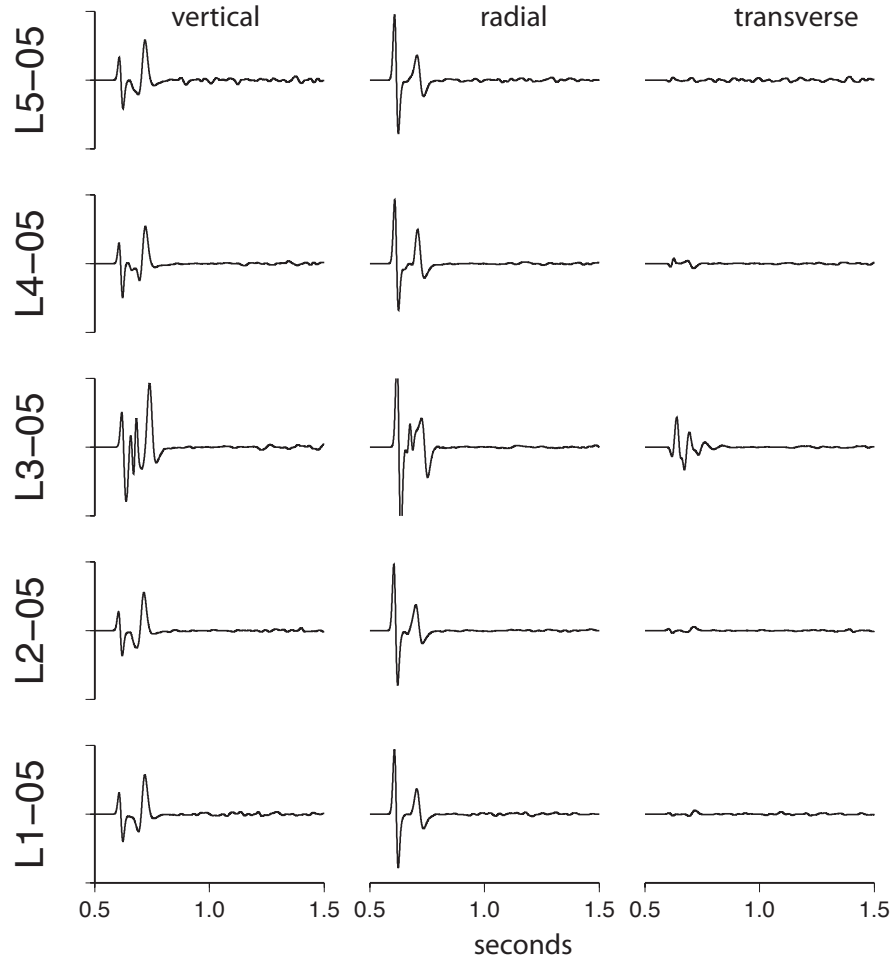


Figure 11. Synthetic seismograms of expected motion using an isotropic explosion source at 0.5 km distance with the revised 3D model, topography, and a node spacing of 5 m. Note prominent transverse energy on L3 line due to scattering.

Figure 11 shows simulations of the SPE2 wavefield at a distance of 0.5 km using an isotropic source and Figure 12 shows the same distance with the GEODYN source. Note that the isotropic source uses an *a priori* seismic moment as source size and does not specifically include any coupling factor while the GEODYN model uses the approximate explosive source and should include coupling between the explosive and the media. Care should be taken in interpreting differences in frequency as the frequency content of isotropic source was specified to avoid numerical effects due to grid size and wavelength; the GEODYN source terms were filtered differently during the interpolation to match the WPP node spacing. We are working on resolving these details. As each simulation requires a full GEODYN run followed by post-processing and then a full WPP simulation, each test is time-consuming. The simulations in this report are the first test of the GEODYN/WPP coupling with a highly heterogeneous far-field model.

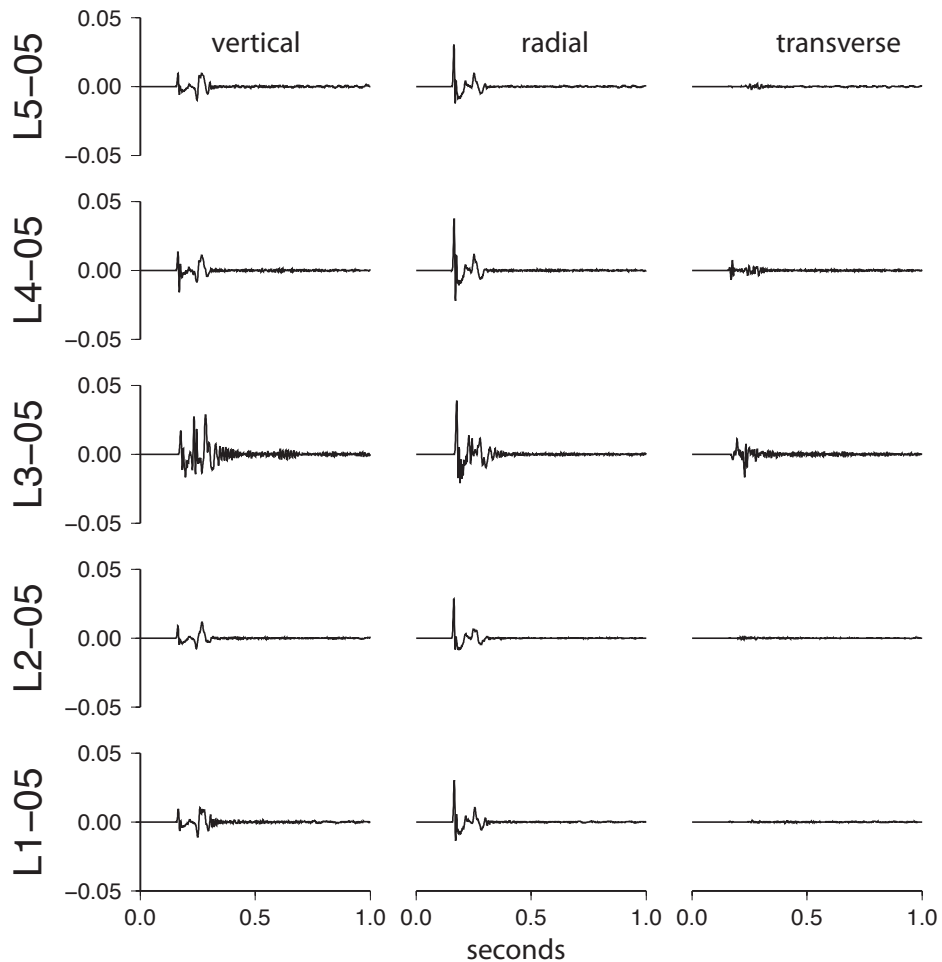


Figure 12. Preliminary synthetic seismograms of expected motion using an embedded GEODYN source (100 m cube) within a WPP model with 3D structure (no topography) and a node spacing of 5 m.

Coupling the two codes has been challenging and therefore simple source models are being tested initially, as these are easier to link with WPP and are useful for

comparison to other models, such as isotropic or CLVD solutions. The GEODYN model used in the current simulation is axisymmetric and hence cannot generate transverse motions. Future improvements are intended to add full 3D sources to the GEODYN source, which will provide a source component of transverse energy. It would be useful at that time to try to match near-field measurements as well as the far-field observations.

In addition to generating seismograms at specific locations, simulations over the entire model space were generated. These are useful in identifying effects of specific geologic features (*Figure 13*). The strong effect of the boundary between the granite of the Climax Stock and the alluvium in Yucca Flat is clearly visible in slowing and amplifying the seismic waves.

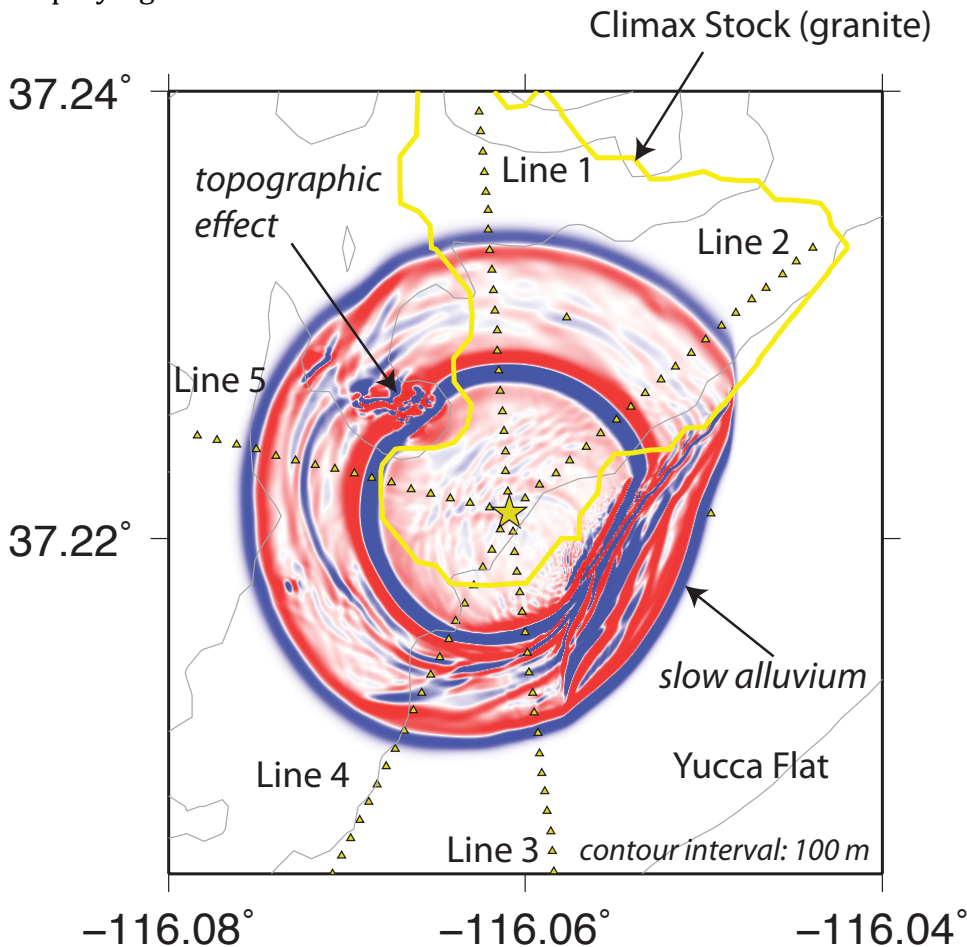


Figure 13. Model of expected SPE2 amplitudes using the refined model.

Rotational components. Recently, low-cost rotational seismic sensors have become available which measure the rotational components of seismic waves [e.g. Lee *et al.*, 2009] as opposed to the traditional components of translational motion. Rotational motions have the potential to provide information on local phase velocities and scattering and partitioning of P and S waves. Nigbor [1994] found significant rotational energy (660 μ rad) at 1 km distance from a 1 kiloton explosion.

As the rotational component is half the curl of the ground velocity, it is straightforward to calculate the expected rotational component from the finite difference models and this has been implemented in WPP. *Figure 14* shows the expected rotational components at 1 km from the SPE2 explosion and a comparison between observed SPE1 rotational waveforms and synthetics. Note that the scaling factor of 0.5 has not been applied to these seismograms and these represent the curl of the ground velocity. The ratio between the transverse acceleration and the rotation rate should yield an estimate of the Love-wave phase relationship at a specific station. The rotation rate should be in phase and the phase velocity should be equal to the transverse acceleration divided by twice the vertical rotation, which is in effect a point measurement of the phase velocity.

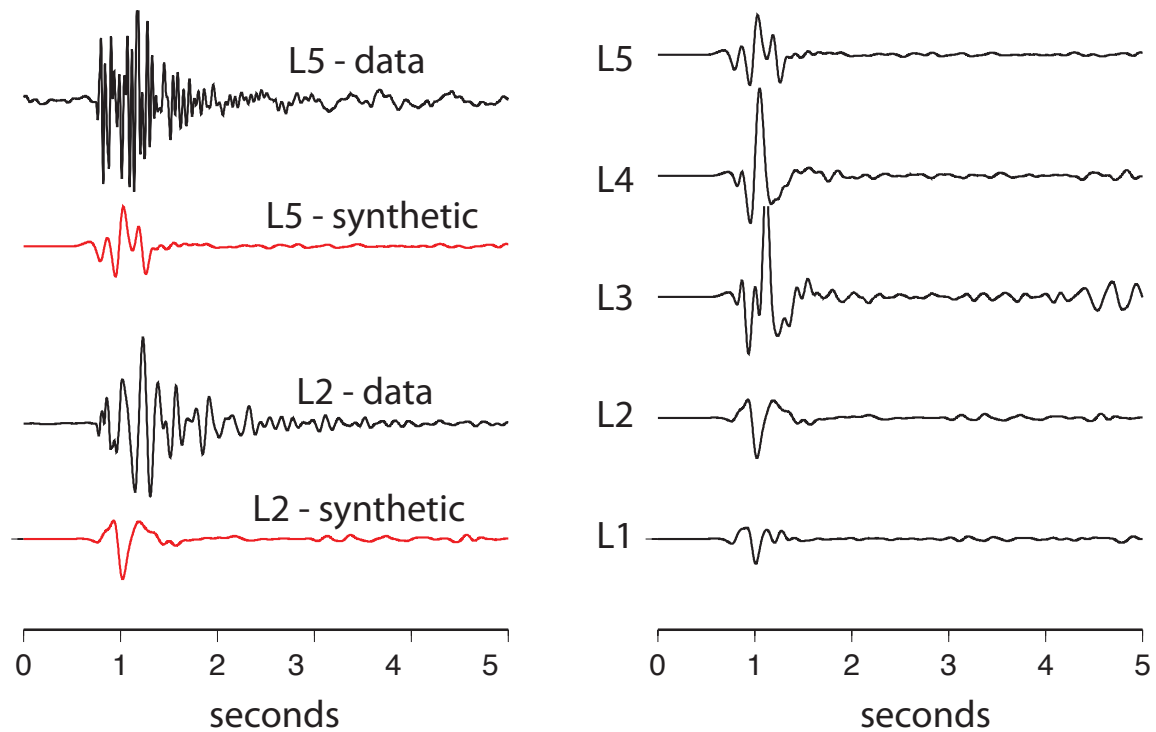


Figure 14. (Right) Comparison of observed SPE1 rotational data (black) at 1 km distance with synthetics (red). Both data and synthetics have been bandpass filtered (1 to 10 Hz). The L5 data appears to have longer period noise visible before the signal. In general, line L5 is predicted to show more complex waveform and this is apparent in the data as well **(Left)**. Synthetic seismograms of expected rotational motion (vertical axis) observed at 1.0 km distance. Note additional complexity on lines 3-5.

Empirically-based amplitudes. A variety of empirically based amplitude relationships have been developed to estimate amplitudes. These tend to vary greatly depending on the site and path. We focus first on amplitudes recorded near (less than 2 km) the shot. Peak velocity amplitudes on the vertical components at a 100 m distance

were on the order of 2 cm/s for the 100 kg SPE1 shot. Assuming square-root scaling, this would predict on the order of 6 cm for the approximately 1000 kg SPE2 shot.

Maximum amplitudes (peak-to-peak, in velocity) as measured at the nearest stations (100 m) were on the order of 2 to 4 cm/s. *Figure 15* shows initial P amplitudes along with expected values derived from a set refraction explosions [Fuis and Kohler, 1992]. Expected values for SPE2 might be expected to lie along the upper red line corresponding to 1000 kg. A question is the amount of coupling between the seismic pad and the surface, as the pads were only shallowly (about 6 inches) buried, which might lead to a pronounced site response.

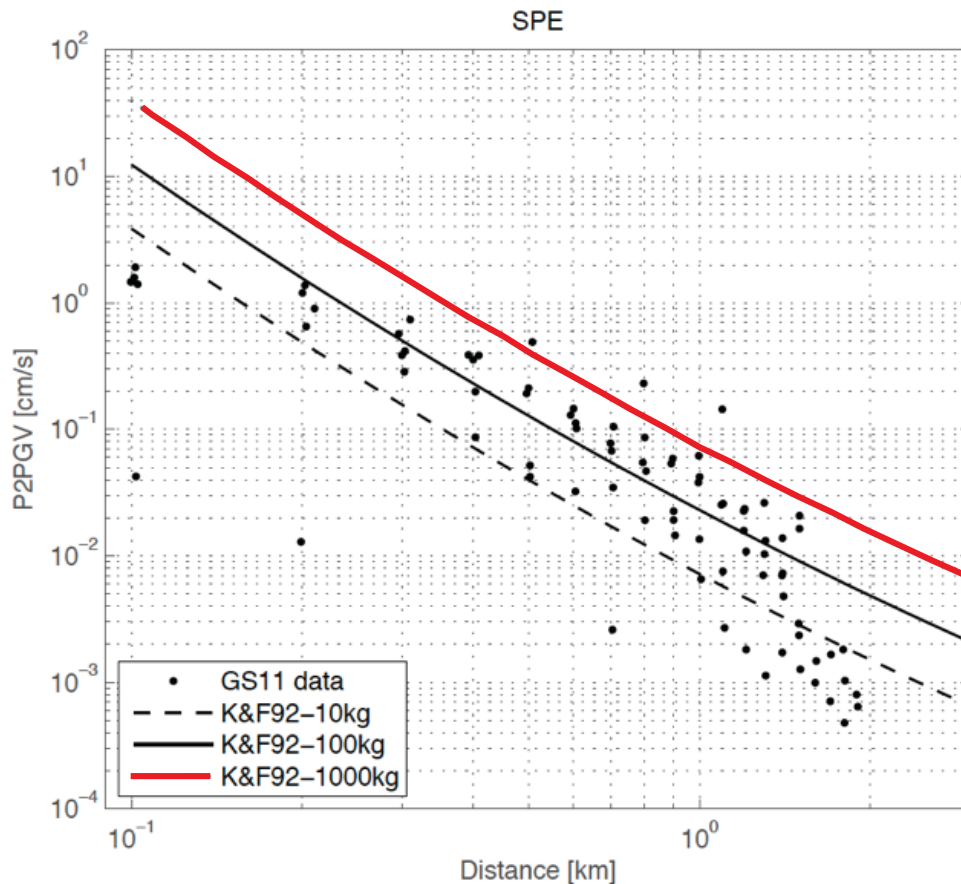


Figure 15. Estimated peak-to-peak amplitudes measured from the first P wave of the SPE1 shot (black dots). Lines indicate values from Kohler and Fuis (1992) and the red line (1000 kg) represents the approximate theoretical values for the SPE2 shot. SPE2 amplitudes should, in theory, be similar to the SPE1 amplitudes shifted upward by the distance between the solid line and the upper red line.

A study by Kohler and Fuis [2002] fit amplitudes using an empirical equation based on a variety of source site types (e.g. water, wet and dry alluvium, hard rock). Figure 15 shows amplitudes measured for SPE1 versus the Kohler and Fuis relationship. The upper dashed line, which represents motion due to a 1000 kg source, shows the

approximate theoretical expected amplitudes for SPE2 after adjusted for any systematic bias between the SPE1 amplitudes and the 100 kg theoretical line. This relationship predicts 0.5 cm/s for SPE2 (peak-to-peak P wave) at 0.5 km distance.

Mueller and Murphy (1971) developed a relationship to characterize source scaling from empirical and theoretical constraints that have been widely applied. Figure 16 shows the expected Mueller-Murphy spectra for both the SPE1 and SPE2 compared with P wave spectra measured from SPE1 at a distance of 1.5 km. The P-wave spectra from the SPE1 shot show excellent signal above the noise between 4 and 100 Hz. Note the expected corner frequency of the SPE1 is around 35 Hz and the expected corner frequency of the SPE2 will be around 15 Hz.

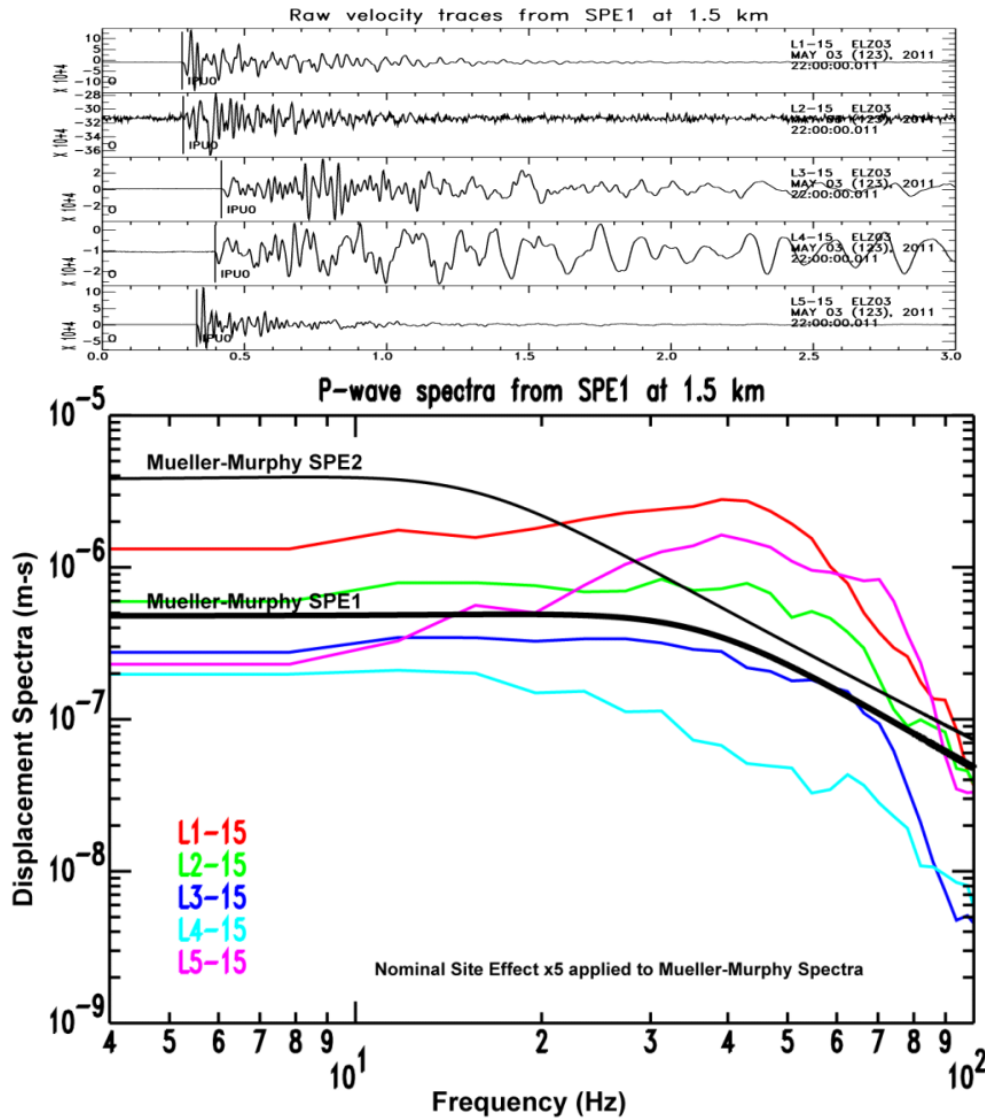


Figure 16. (Top) Seismograms recorded at a distance of 1.5 km. (Bottom) Corresponding P-wave spectra compared with the expected Mueller-Murphy model at 1.5 km for both the SPE and SPE2 shots. Amplitudes for L2-15 are believed to be biased due to possible instrumental problems and may be inaccurate at high frequencies.

As can be clearly seen in *Figure 16* the observed SPE1 spectral amplitudes are quite variable despite the fact that stations are all the same distance from the source. This indicates significant path and site effects as well as the possibility of non-isotropic source effects. We believe that the site effects are likely severe and the largest source of amplitude variability since the sensors were emplaced directly on the surface and not buried and tied to bedrock. In the frequency range from 30-80 Hz there is an almost two order of magnitude variation in the amplitudes between the stations compared to what is expected from the isotropic model.

The planned detonation of the SPE2 shot will allow us to look at relative behavior between tests at stations in common where shared terms such as path and site effects cancel out. For example we will be able to directly test if the predicted Mueller-Murphy spectral amplitude ratio is consistent with the data by looking at the observed ratio without having to know and model the site and path effects. We can also do the inverse and predict the SPE2 signal under the assumption that the isotropic Muller-Murphy P-wave spectral model is correct. We do this by multiplying the observed SPE1 amplitude spectra at a given station by the ratio of the Muller-Murphy SPE2 to SPE1 spectral amplitude. This simulated SPE2 amplitude spectrum is then combined with the original phase spectra and inverse Fourier transformed to create the simulated seismogram at that station.

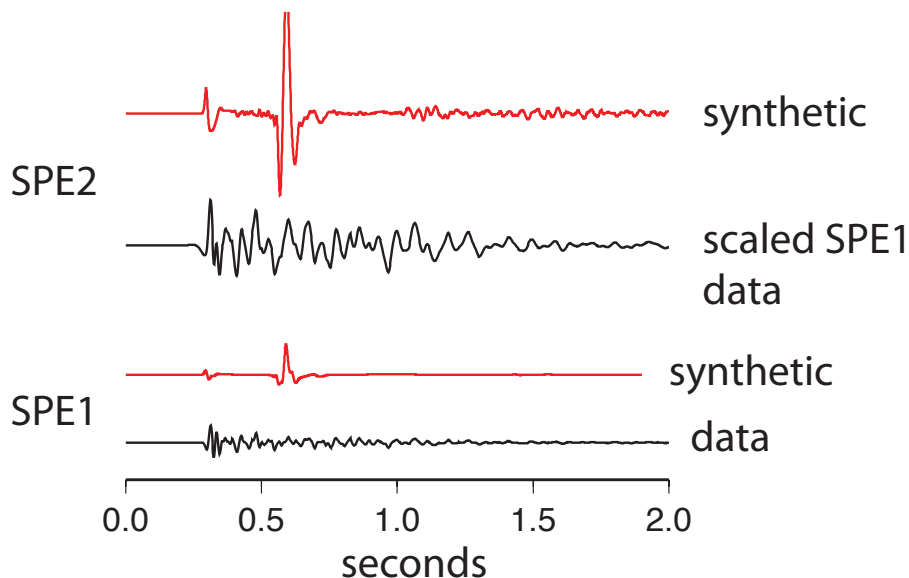


Figure 17. Comparison of SPE1 synthetic and data (bottom, red and black) with scaled SPE1 using spectral ratio based on Mueller-Murphy scaling for the SPE2 (top, black). Top red line is synthetic for SPE2. All on same scale.

Figure 17 shows the broadband SPE1 data at station L1-15.CLZ, 1.5 km away from the source on Line 1, and the simulated SPE2 seismogram at same station. Note the SPE2 amplitudes are larger and shifted to lower frequencies as expected from the spectral models shown in *Figure 16*. We can compare these traces to our physics-based simulations as shown in *Figure 17*. Differences between the synthetics and

this data based simulation reflect unmodeled path and site effects as well as the difference between the isotropic Mueller-Murphy source and the non-isotropic GEODYNE source. For example it is clear that the Rg amplitudes, which are the second arrival in the synthetic calculations are too large and coherent compared to the data, reflecting the need to include more scattering heterogeneities and perhaps near surface attenuation in our Earth models. The ability to model ratios of multiple SPE shot data and synthetics will help us sort out source from propagation effects allowing us to develop better modeling capabilities.

Aftershock prediction. Aftershocks are one means of discriminating between underground explosions and earthquakes [Ford and Walter, 2010] and passive monitoring for aftershocks is included in the Comprehensive nuclear-Test-Ban Treaty to refine the search area and to resolve the nature of an event [e.g. www.ctbto.org, 2011]. The seismic network will continue continuous recording of data for two weeks after the SPE1 shot, allowing an investigation of aftershock activity, so here we provide an estimate of the expected aftershock probabilities based on our NTS models.

The SPE2 is approximately 1 ton TNT explosion and using *Khalturin et al.* [1998] magnitude-yield relationship, $M = 2.45 + 0.73 \log_{10}(W [t_{\text{TNT}}])$, gives a mainshock magnitude (Mm) of 2.5. Using an aftershock model derived from BENHAM (Pahute Mesa) and magnitude of detection (Md) thresholds of -0.5, 0, and 0.5 (differential magnitude = 3, 2.5, and 2, respectively) we can estimate the probability of at least one aftershock occurring at or above a given Md within a given duration beginning after the explosion. Details of the aftershock prediction model can be found in *Ford and Walter* [2010].

The probabilities are given in *Figure 18* where, for example, there is a 92% probability that within 2 weeks there will be at least one aftershock with magnitude greater than a detection threshold of 0.

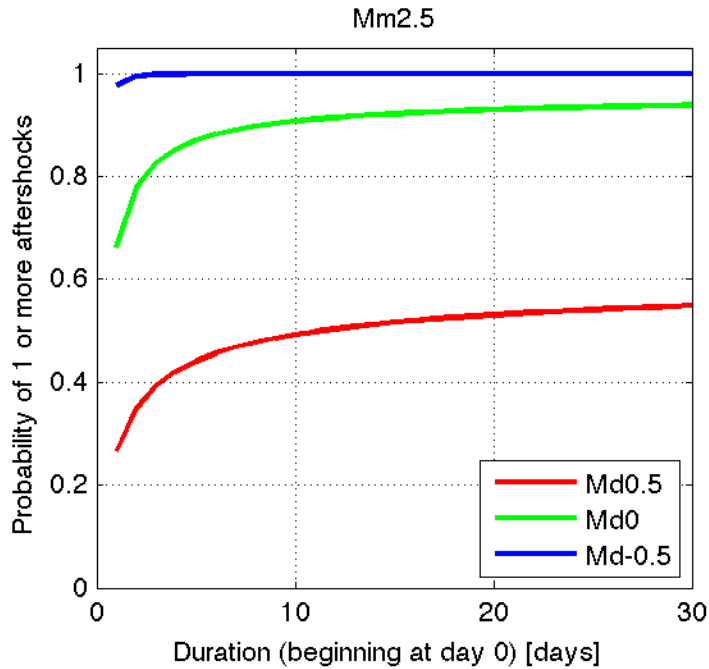


Figure 18. *Aftershock probabilities using the NTS hard-rock model for a mainshock magnitude (M_m) of 2.5 and several detection magnitudes (M_d).*

We can also use the model to predict the expected number of aftershocks above a given detection magnitude at an assumed probability (P) within a given duration. The expected number of aftershocks is given in Figure 19 where, for example, at a probability of 0.5 we can expect four aftershocks above $M-0.5$ within one day and six aftershocks within a week.

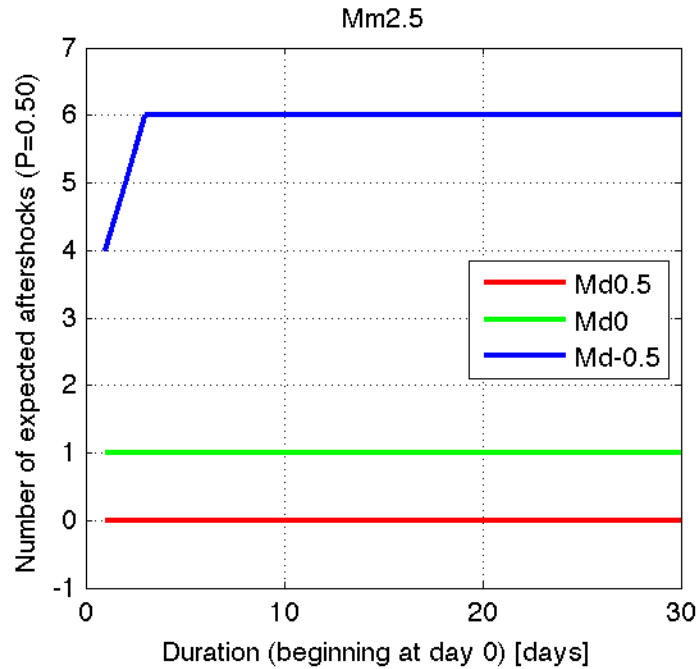


Figure 19. *Expected number of aftershocks using the NTS hard-rock model at a probability of 0.5 for a mainshock magnitude (Mm) of 2.5 and several detection magnitudes (Md).*

Climax Stock is harder than Pahute Mesa welded tuff so we use a hard-rock model derived from a shot at STS (Balapan) and recalculate the probabilities. *Figures 19 and 20* show the probabilities and expected number of aftershocks for this hard-rock model. *Figure 20* shows that at seven days the probability of detecting at least one aftershock above M0 is near 1. *Figure 21* shows that within three days after the mainshock we can expect two aftershocks above M0 at P=0.5.

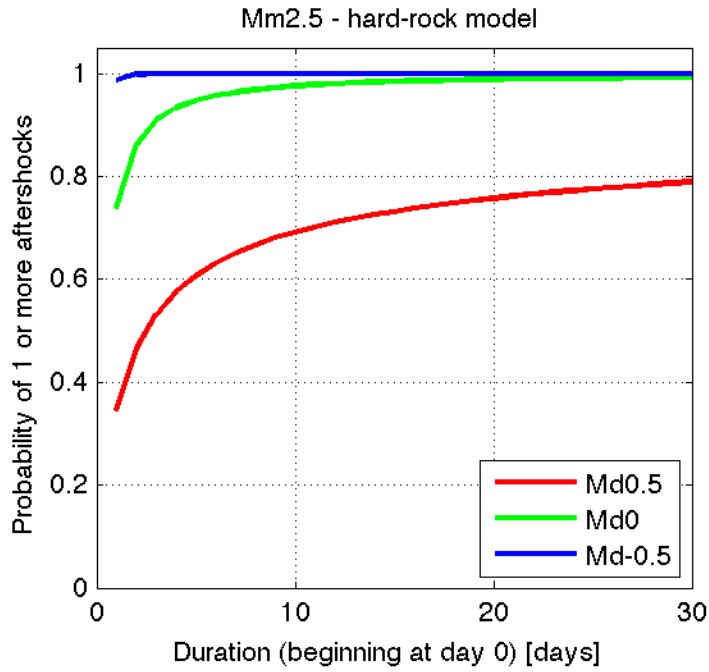


Figure 20. *Aftershock probability using hard-rock model*

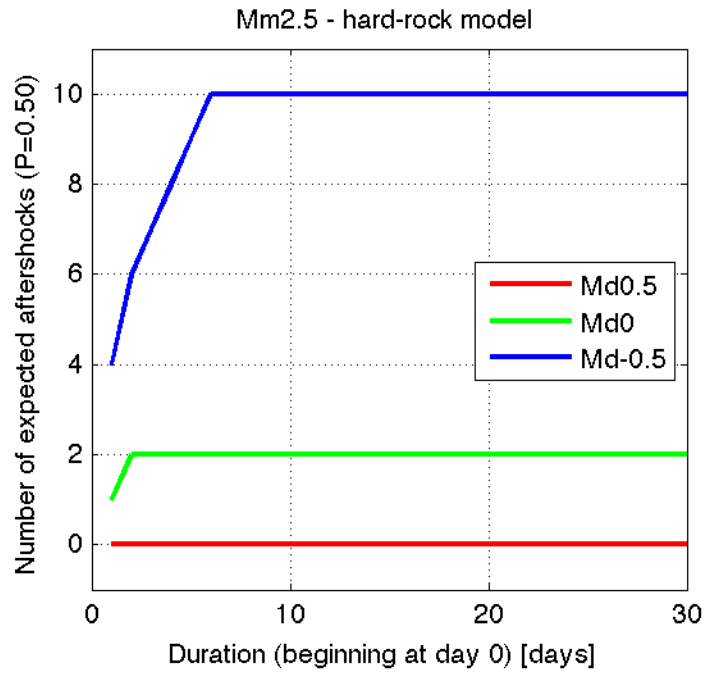


Figure 21. *Expected number of aftershocks using hard-rock model*

Conclusions and recommendations. This report summarizes results from previous SPE shots and observations and, based on these results as well as additional capabilities, provides a set of predictions for the SPE2 shot.

The SPE1 pre-shot simulations matched the overall preliminary expectations reasonably well. Strong effects from lateral heterogeneities in the subsurface were observed including high amplitudes and slower wavespeeds in Yucca Flat, as expected. Transverse energy was expected on paths to the south and east of ground zero and this was observed, although the models underestimated the amplitude and significant transverse energy was observed within the granite block itself. Surface wave amplitudes on lines to the south and east were poorly fit and likely due to artificially high shear wave velocities in the model forced by computational constraints. Velocities within layers, especially the granite, were not matched exactly.

A major challenge appears to be matching the transverse energy visible in the data, which is likely due to a combination of source and path effects. In fact, determining the partitioning of shear waves due to source and path is one of the primary goals of this experimental series. While the current synthetics generate significant transverse energy due to scattering along various lines, we have not yet included a source capable of generating transverse energy in the synthetics.

A number of improvements as well as new capabilities were added for the SPE2 predictions. The velocity model was revised to match traveltimes and the layer model expanded in area. The most significant improvement, although still at a preliminary stage, was the addition of new source modeling capabilities to the WPP model. By embedding a source generated by a hydrodynamic modeling package (GEODYN) within the far-field (WPP) model, a sophisticated near-source model that includes nonlinear effects can be included. This represents a significant step forward from the previous source representations and allows for estimates of amplitudes. In addition to the improvements in the source, the capability to generate simulating rotational motions was also added for comparison with rotational measurements. Finally, an estimate of expected aftershock probabilities and rates was generated for SPE2 using methodology of *Ford and Walter [2010]*.

Future improvements:

- Additional refinements of the velocity model based on gradients measured from boreholes and possibly the addition of more layers.
- Apply corrections based on ambient noise cross-correlation.
- Revise model of granite block to include weathered layer.
- Refine GEODYN/WPP coupling should improve amplitude estimates and improve the simulations.
- Testing of CLVD source models.
- Compare simulations of rotational data with observed data
- Improve visualization of the simulations for rapid assessment.

Acknowledgements.

We thank the DOE Office of Sciences, OSCR and the LDRD for support of WPP. A Computing Grand Challenge provided support for the computational resources. We appreciate the efforts of NSTec personnel for efforts in conducting the SPE experiment and collecting the seismic data.

This work performed under the auspices of the U.S. Department of Energy by Lawrence Livermore National Laboratory under Contract DE-AC52-07NA27344.

LLNL contribution #

References.

- Antoun, T. H., I. N. Lomov, and L. A. Glenn (2001). Development and application of a strength and damage model for rock under dynamic loading, in proceedings of the 38th U.S. Rock Mechanics Symposium, Rock Mechanics in the National Interest, D. Elsworth, J. Tinucci and K. Heasley (eds.), A. A. Balkema Publishers, Lisse, The Netherlands, 369–374.
- Antoun, T. H. and I. N. Lomov (2003). Simulation of a spherical wave experiment in marble using multidirectional damage model, 13th American Physical Society Topical Conference on Shock Compression of Condensed Matter, Portland, OR July 20–25, 2003.
- Antoun, T. H., I. N. Lomov and L.A. Glenn (2004). Simulation of the penetration of a sequence of bombs into granitic rock, *Int. J. Impact Eng.* 29: 81–94.
- Ford, S. R., and W. R. Walter (2010) Aftershock characteristics as a means of discriminating explosions from earthquakes, *Bull. Seis. Soc. Amer.* 100(1), 364-76, doi: 10.1785/0120080349.
- Geotechnical Sciences Group, (2006), A Hydrostratigraphic Model and Alternatives for the Groundwater Flow and Contaminant Transport Model of Corrective Action Unit 97: Yucca Flat-Climax Mine, Lincoln and Nye Counties, Nevada, DOE/NV/11718—1119.
- Khalturin, V. I., T. G. Rautian, and P. G. Richards, (1998), The seismic signal strength of chemical explosions, *Bull. Seismo. Soc. Amer.*, V88, 6, 1511-1524.
- Kohler, W. M. and G. S. Fuis, (1992), Empirical dependence of seismic ground velocity on the weight of explosives, shotpoint site condition, and recording distance for seismic refraction data, *Bull. Seismo. Soc. Amer.*, 82, (5), 2032-2044.

- Lomov, I. N., T. H. Antoun, J. Wagoner and J. Rambo (2003). Three-dimensional simulation of the Baneberry nuclear event, in Proceedings of the 13th American Physical Society Topical Conference on Shock Compression of Condensed Matter, Portland, OR July 20–25, 2003.
- Nigbor, R. L. (1994). Six-degree-of-freedom ground motion measurement, *Bull. Seismol. Soc. Am.* 84, 1665–1669.
- Mellors, R. J., P. Harben, S. Ford, J. Wagoner, B. Walter, A. Rodgers, T. Hauk, S. Ruppert, S. Myers, E. Matzel, D. Dodge, M. Pasyanos, R. Gok, N. Simmons, A. Petersson, B. Sjogreen, and J. P. Lewis, (2011a), SPE 1 Data Quicklook report, LLNL-TR-485228.
- Mellors, R. J., P. Harben, S. Ford, J. Wagoner, B. Walter, A. Rodgers, T. Hauk, S. Ruppert, S. Myers, E. Matzel, D. Dodge, M. Pasyanos, R. Gok, N. Simmons, A. Petersson, B. Sjogreen, and J. P. Lewis, (2011b). Analysis and simulation of far-field seismic data from the source physics experiment explosions, 2011 Monitoring Research review: Ground-Based Nuclear Explosion Monitoring Technologies, Sept. 13-15, Tuscon, AZ, LA-UR-11-04823, p. 503-511.
- Mueller, R. and J. Murphy (1971). Seismic characteristics of underground nuclear detonations Part 1: Seismic source scaling, *Bull. Seismol. Soc. Am.* 61: 1675–1692.
- Petersson, N. A. (2011). WPP software website, <https://computation.llnl.gov/casc/serpentine/software.html>
- Petersson, N. A. and B. Sjogreen (2009). An Energy Absorbing Far-Field Boundary Condition for the Elastic Wave Equation, *Comm. Comput. Phys.* 6: 483–508.
- Petersson, N. A. and B. Sjogreen (2010). Stable and efficient modeling of anelastic attenuation in seismic waves, submitted to *Comm. Comput. Phys*, LLNL-JRNL-460239.
- Petersson, N. A. and B. Sjogreen (2011). User's guide to WPP version 2.1, Lawrence Livermore National Laboratory technical report, LLNL-SM-487431.
- Rodgers, A. J., H. Xu, I. N. Lomov, N. A. Petersson, B. Sjogreen, O. Y. Vorobiev and V. Chipman, (2011) Improving ground motion simulation capabilities for underground explosion monitoring: coupling hydrodynamic-to-seismic solvers and studies of emplacement conditions, 2011 Monitoring Research review: Ground-Based Nuclear Explosion Monitoring Technologies, Sept. 13-15, Tuscon, AZ, LA-UR-11-04823, p. 363-371.

Sjögreen, B. and N. A. Petersson (2010). Stable grid refinement and singular source discretization for seismic wave simulations, *Comm. Comput. Phys*, LLNL-JRNL-419382.

Suryanto, W., (2006), Rotational motions in seismology, theory and application, Ph.D dissertation, pp. 118, University of Munich.